Defect tolerance of π-conjugated polymer crystal lattices and their relevance to optoelectronic applications

Wesley K. Tatum,[1] Anton B. Resing,[1] Lucas Q. Flagg,[2] David S. Ginger,[2] Christine K. Luscombe[1,2,3]*

[1]Department of Materials Science and Engineering, University of Washington, Seattle, WA 98195-2120, USA

[2]Department of Chemistry, University of Washington, Seattle, WA 98195-1700, USA

[3]Department of Molecular Engineering and Sciences, University of Washington, Seattle, WA 98195-1652, USA

Keywords: π-Conjugated Polymers/Crystallization/Defects/Nanowires/Self-Assembly/

Abstract: This work seeks to understand the role of structural defects in the polymer chain on the crystallization and crystal lattice of π-conjugated polymers, which is crucial for being able to predict morphology and performance of π-conjugated polymer active layers in optoelectronic devices. Such a crucial understanding of device performance has been difficult to establish, however, in this work self-assembled nanowires of poly(3-hexylthiophene) (P3HT) are used in order to reduce analytical contributions from amorphous domains, allowing a more direct path to

probe the effect of regio-defects and chain end-groups on the crystal lattice. Using P3HT synthesized to have precisely varied defect concentrations, it was demonstrated that these defects can be incorporated into the crystal lattice, particularly regio-defects. However, this incorporation comes with a decrease in electronic properties as a result of diminished short-range order and lattice distortions. Bulky end-groups can be incorporated into the lattice, although there is a preference for their exclusion. However, the use of π-π interacting end-groups, such as toluene, is shown to mitigate disruption to the crystal lattice that result from the end-group incorporation. In fact, π-π interacting end-groups seem to promote long-range order and crystal growth. Additionally, it was found that tuning the molecular weight of the polymer to an integer multiple of the observed width of the crystal lamellae, l_c, can increase the enthalpy of fusion, ΔH_f, for the crystal by as much as 20% by facilitating the exclusion of end-groups from the crystal lattice. These results demonstrate that π-conjugated polymer crystal lattices have a high tolerance for disruptions to short-range order so that long-range order can be preserved. Further, this study underscores the need to consider structural defects in polymer chains and their consequences on the crystal lattice during the design and implementation of π-conjugated polymers.

INTRODUCTION

π-Conjugated polymers (CPs) have seen rapid development since their discovery in the 1970s and, within the past decade of research, key insights have brought them to the cusp of commercial implementation.[1,2] Flexible and stretchable field-effect devices, sensors, and thermoelectric devices that are based on these materials have seen significant improvement, and lab-scale CP-based solar cells have demonstrated power conversion efficiencies beyond 14%.[3-8] Despite these landmarks, there are still problems that need to be addressed before reproducible, efficient, and effective products can be fully realized.

Although synthetic precision has drastically improved in the past years, defects in the chemical structures of CP are difficult to completely avoid.[9,10] Common imperfections, such as coupling defects during polymerization, dispersity in molecular weight, and end-groups, can disrupt crystallization and thereby affect many different material properties, including charge transport and mechanical stiffness. Such properties are also affected by processing conditions, which is beyond the scope of this study. The effects of chemical defects have been the subject of some study, particularly coupling defects.[11–16] In asymmetric monomer containing homopolymers, such as poly(3-hexylthiophene) (P3HT), this is defined as regioregularity (RR), which is the percentage of monomers coupled in the preferred head-to-tail (HT) conformation, rather than head-to-head (HH) or tail-to-tail (TT) conformations (Figure 1).

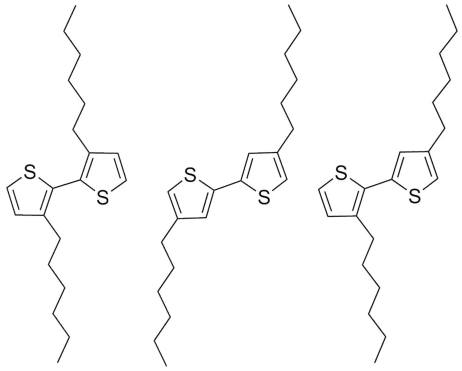

Figure 1. Regio-defects in P3HT: (left-to-right) HH and TT coupling, compared to the preferred HT coupling.

In order to relieve the steric interactions of the bulky side-chains, the incorrectly coupled monomers twist into a more *gauche* alignment, which reduces their p_z orbital overlap and disrupts π-conjugation along the backbone. This twist also reduces the ability of that polymer chain to pack closely with other chains, disrupting the crystal lattice and reducing crystallinity; such disruptions in crystallinity and orbital overlap are detrimental to charge conduction pathways in optoelectronic

devices.[17–19] Coupling defects in donor-acceptor (D-A) copolymers can also include homo-couplings, which are beyond the scope of this investigation. Dispersity (*Đ*) in the molecular weight profile of the CP has been shown to also drastically reduce crystallinity because short chains have a higher concentration of end-groups per crystallizable monomer unit when compared to longer chains. What's more, CP of drastically different molecular weights have a tendency to crystallize differently, both with regards to crystal lattice dimensions and mechanism.[14,15,20–23] Finally, the effects of end-groups seem to be dependent on the type of end-group that is used. For instance, Kim *et al.* have shown that thin films of CPs with Br as an end-group have far less crystalline order than thin films from the same CP but with thiophene end-groups.[24] As seen in Figure 2, the common end-group, Br, has a van der Waals diameter of 0.37 nm, approximately the same size as the π-π stacking distance in P3HT, 0.38 nm. The introduction of this steric bulk disrupts close packing and, therefore, polymers with larger end-groups tend to have less order.[25–27] However, Koldemir *et al.* have shown that, despite being relatively large, toluene end-groups can actually serve to promote a higher degree of order in CP thin films than the same CP capped with H, the smallest possible end-group.[28] This was attributed to stronger aggregation in solution for the polymer capped with toluene-H end-groups.

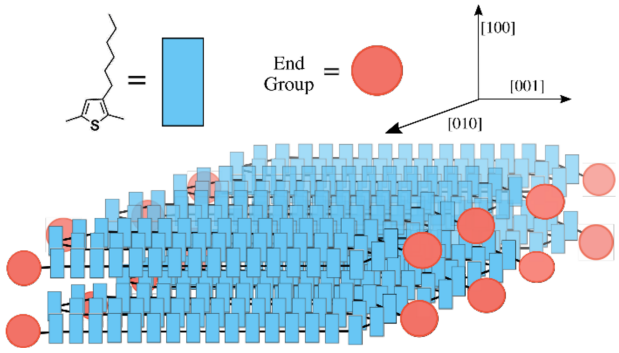

Figure 2. A representative diagram of a CP crystallite. Bulky end-groups can be similar in size to the intermolecular distance, which is disruptive to crystal growth.

It seems apparent that the disruption of electronic properties and device performance and order tends to increase with the number of chemical structure defects in CP chains cast in thin films for devices, and further that these effects come as a result of changes in crystallinity and short-range order. Despite this, there have been relatively few investigations into understanding precisely why this occurs and where these defects reside in the thin film or how their location can be manipulated. In other words, there has been little investigation into how or why the defects affect the crystallinity. This is not the case for traditional, non-conjugated polymers, as an investigation into the role of chemical defects in crystallization began with a reformulation of the Thomson-Gibbs equation in 1955 by Flory.[29] The resulting equation described an ideal crystalline state that excluded defects completely into the surrounding amorphous domains so that the crystal lattice is preserved. In this ideal case, increasing the defect concentration also increases the amorphous fraction of the film as a result of more polymer being excluded from the crystals. This, in turn, decreases the crystal lamellar thickness, l_c. So, the melting temperature, T_m, is depressed by an increasing defect concentration. Later, Sanchez and Eby further reformulated the Thompson-Gibbs equation to describe the more common case, where there is partial inclusion of defects into the crystal lattice, which tends to occur in kinetically limited processes.[30] Their reformulation includes an enthalpic penalty for the incorporation of defects, which distorts the crystal lattice and reduces intermolecular interactions, thereby lowering the enthalpy of formation, ΔH_f, for the crystal. In this model, T_m is decreased with increasing defect concentration as a result of both decreasing l_c and diminishing ΔH_f.

In the past few decades, researchers have developed a much deeper understanding of the crystalline behavior of non-conjugated polymers. In particular, polyethylene (PE) has been the subject of much research. This is due to a few reasons, namely, PE is one of the simplest possible

polymer structures. This drastically simplifies analytical techniques like X-ray diffraction (XRD) or nuclear magnetic resonance (NMR), where increased structural complexity can cause increased complexity of signals produced, and also reduces computational complexities for simulations. Additionally, PE is of high interest for industrial purposes and highly precise polymerizations have been developed, which have allowed for detailed structure-property relationships to be constructed; phase diagrams of PE at different pressures and varied temperature and M_n have been developed, as just a few examples.[31,32] The crystal structure of PE throughout ranges of operating conditions and polymer profiles (e.g. M_n, $Đ$, etc.) have been systematically developed and corroborated. What's more, in-depth studies of local variations in crystallinity have shed light on semicrystalline polymer behavior.[33,34] Such an intimate knowledge of PE has been a significant achievement that has improved the implementation and understanding of PE and other non-conjugated polymers. For CPs, it has been difficult to even simply evaluate which defects are incorporated into the crystal lattice and the extent of their incorporation. This is because of the difficulties associated with producing CP samples that have a range of discrete defect concentrations, and difficulties in analyzing the highly interconnected semicrystalline thin film structure of polymers.[2,35]

The complex nanostructure of polymer thin films is exemplified in Figure 3, which shows highly anisotropic, lamellar domains of crystalline polymer separated by amorphous domains that conform to Flory's model of complete exclusion of defects from the crystal lamellae.[36] According to that model, all the defects in the chemical structure, which are listed in Figure 3, would be excluded to or transported to the amorphous domains to preserve the short-range order of the crystal lattice. In the context of CP, this means that regio-defects and end-groups would be expected to be excluded in such a model. Conversely, some or all types of defects could be

incorporated into the crystal lattice in the model outlined by Sanchez and Eby. Because of the complex morphology of these thin films, it has been difficult to determine which model most accurately describes CP. In order to reduce the complexity of the CP morphology, we used self-assembled nanowires of P3HT that were produced through the whisker method.[37] The precipitation of these nanostructures from a poor solvent is a kinetically limited process, meaning that it can still be used to probe the aggregation and close-packing of thin films produced using faster processing methods, such as spin-coating or blade-coating. However, the polymer chains in the nanowires are also able to reach a much more thermodynamically stable conformation because they age in solution for up to 72 hours, as presented in this investigation. The use of these nanowires allows for the examination of an upper threshold in the kinetically limited defect tolerance of crystalline domains, with minimal interference from amorphous domains. In order to precisely alter the defect concentration, we utilized our previously established synthetic routes for producing P3HT with high control over RR, molecular weight, $Đ$, and end-groups.[9] This allows for nanowires to be made from P3HT with a range of defect concentrations and to have the resulting crystal structure examined. By examining different series of nanowire samples, we were able to identify the location of regio-defects and end-groups in highly ordered structures and elucidate the connections between the defects and their effects on material properties in a generalized manner.

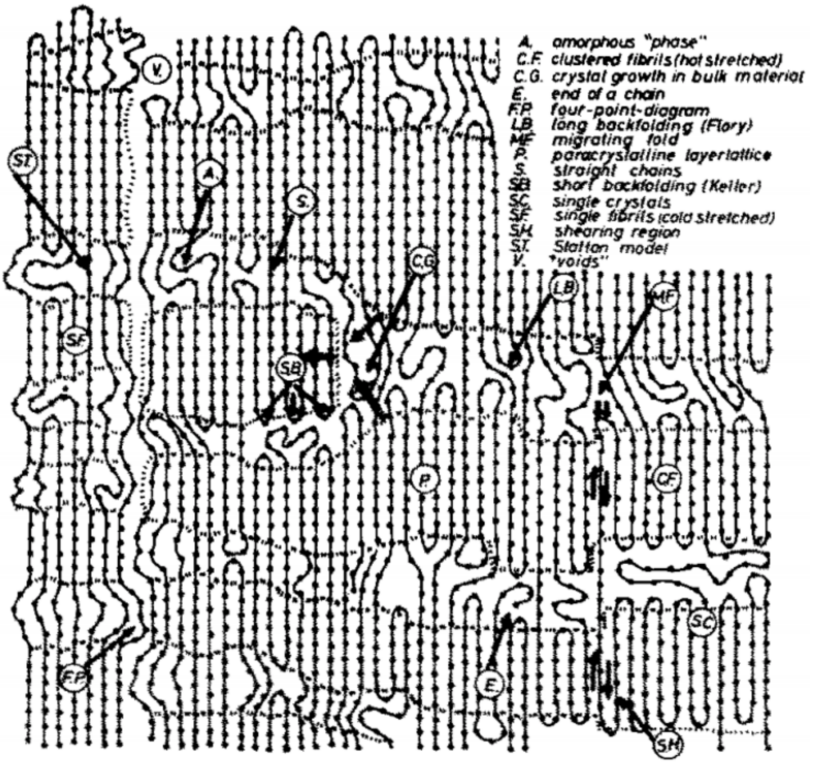

Figure 3. A top-down view of thin film morphology for traditional polymers following Flory's model of complete exclusion, with lamellar crystalline domains separated by amorphous domains and the defects only residing in the amorphous domains. As shown in this figure, the amorphous regions (A) contain all of the chemical defects, including short backfolds (SB), long backfolds (LB), chain ends (E), voids (V), migrating folds (MF), and Statton model (ST) defects, as well as the beginnings of new crystallites (CG). Depending on processing, crystalline domains can be single fibrils (SF), clustered fibrils (CF), paracrystalline layerlattice (P), or single crystals (SC). Shown also are shearing region defects (SH) to the crystal lattice. Reproduced with permission from ref 36. Copyright 1963 AIP Publishing LLC.

RESULTS AND DISCUSSION

In our prior work, we had shown that nanowires can be successfully created using P3HT that has RR as low as 93% with bulky Br end-groups, which is considered to be a higher defect

concentration than desired for many device applications.[17] Increasing the RR was shown to promote the crystal coherence in the π-π direction, but the location of these defects in the nanowire structure was not investigated. As shown in Figure 4, there are two nanowire structures that could be expected to form. Model A follows Flory's model and assumes that all of the defects are being excluded to the perimeter of the nanowire, where the amorphous domain is expected to exist. If this case is the correct description, then it follows that increasing the concentration of defects would decrease l_c and increase l_a as more polymer is excluded from the crystalline domain. This differs from model B, where some defects are incorporated directly into the crystal lattice at the expense of the ΔH_f for the crystal, as described by Sanchez and Eby. In this case, l_c would vary significantly less than in model A and the total width of the nanowire would remain the same, since the increase in the amorphous fraction of the nanowire would be diminished by defect inclusion. So, if both l_c and the width of the nanowire (l_c+l_a) remain constant, then model B would correctly describe the treatment of defects by the crystal lattice.

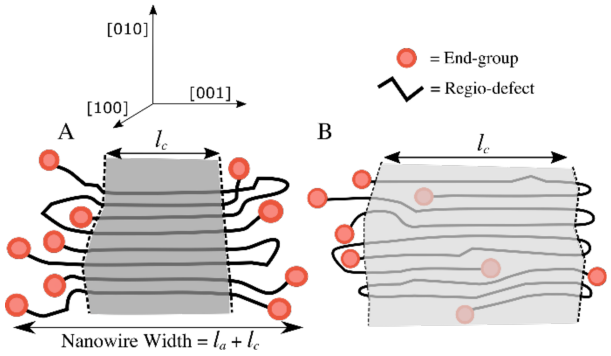

Figure 4. Proposed nanowire structures for the cases where there is either (A) complete exclusion of defects or (B) partial inclusion of defects into the crystal lattice. Darker grey indicates higher crystallinity.

As an initial investigation into defect tolerance at high defect concentrations, nanowires were formed from commercially available P3HT, following the procedure outlined in the supporting

information. In order to identify the preferential inclusion or exclusion of defects during nanowire formation, the P3HT that was unincorporated into the nanowire, which remained in solution during centrifuging, was analyzed and compared to the nanowire incorporated P3HT. As seen in Figures S1-S7 and summarized in Table S1, the nanowire self-assembly process tends to exclude polymers with RR below ~90%. This is assumed to occur because chains with lower RR present too many backbone torsions to successfully fold and close-pack with other chains in such a highly ordered nanostructure.[38] Similarly, there was a decrease in the number of Br end-groups that were incorporated into the nanowires. This is identified by a suppression of the Br-H peaks in the MALDI-TOF spectra shown in Figures S8, S10, and S12 compared to Figures S9, S11, S13, and S14. This is summarized in Table S1, where it is apparent that there is a much smaller Br-H:H-H end-group ratio for the nanowire incorporated P3HT than the unincorporated and as-purchased P3HT. Finally, there was an exclusion of chains with a degree of polymerization (DP) of less than approximately 50 monomer units. Interestingly, this apparent threshold corresponds to l_c as determined by differential scanning calorimetry (DSC) and outlined in Table S1. The observed tendency to incorporate integer multiples of l_c will be explored to a greater extent below. The SEC analyses of these nanowires seem to indicate preferential exclusion of long chains from the nanowire, however, the most likely explanation for this result is that the longest chains were not solvated adequately by the anisole, which is an intentionally poor solvent for P3HT, during the self-assembly process, inhibiting their participation in nanowire formation. These results complement the findings of Roehling *et al*., which identified the preference to exclude smaller chains during nanowire formation, in part to reduce end-groups in the nanowire structure.[38] As the aging progressed, there was a noticeable increase in the ΔH_f of the nanowires, which is attributed to the increased time to approach a thermodynamically preferred, highly crystalline state.[38] Despite

this increase in the crystallinity, there was no observed increase in l_c, as determined by the Broadhurst equation (Equation 1) and the peak melting temperature, located using DSC (Figure S15).[21]

$$T_m = T_m^o \frac{n+a}{n+b} \qquad (1)$$

In the above equation, T_m is the observed melting temperature peak, T_m^o is the melting point of an infinite crystal of P3HT, n is the number of repeat units the crystal is wide in the [001] direction, and a and b are constants. In addition to constant l_c, there was no observable difference in the heights or widths of the nanowires, as measured by AFM (Figure 5), nor in the coherence in the [010], π-π stacking direction, $\xi_{(010)}$, as determined by Scherrer analysis of the XRD spectra shown in Figures S17-S19.

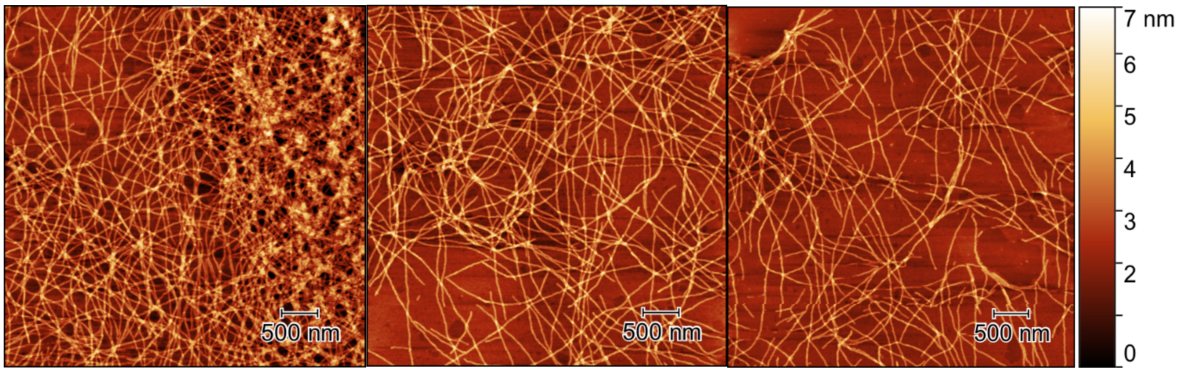

Figure 5. A representative PeakForce AFM image of P3HT nanowires that are aged (left-to-right) 24, 48, and 72 hours. Scale bars are all 500 nm. As seen in these height scans, and described in Table S1, there are no differences in the dimensions of the nanowires in these three different samples.

So, despite the fact that there is inclusion of defects into the nanowire structure at different concentrations for the different aging times, there are no observed differences in the dimensions of the nanowire nor in l_c. This lack of variation in the width of the nanowires and l_c occurs despite

differences in ΔH_f, which is illustrated clearly in Figure 6, which plots nanowire width and l_c as well as ΔH_f as a function of nanowire age.

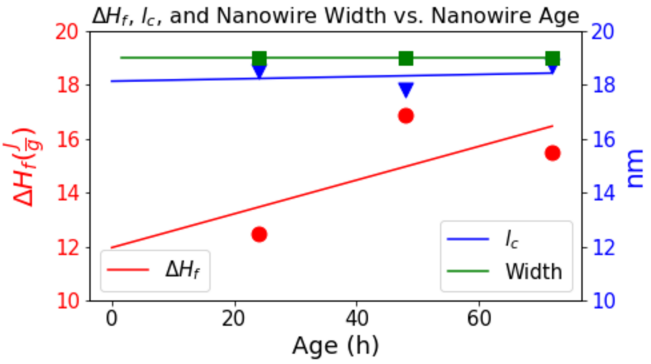

Figure 6: A plot demonstrating that, despite differences in the crystallinity that result from varied defect concentrations, there is little difference in the nanowire widths and l_c for the different samples. Linear fits provide visual guides for the data. Error in the data is associated with instrumental precision. These results are more completely shown in Table S1.

The fact that nanowire width and l_c remain constant, despite clear differences in defect concentration and ΔH_f demonstrates that regio-defects and bulky end-groups can be incorporated to some degree in the nanowire crystal lattice. These defect-induced distortions in the crystal lattice are evidenced in the UV-vis absorption profiles across the different nanowire ages, as show in Figure 7. In order to evaluate the different levels of lattice distortions and the relative degrees of *H*-like and *J*-like coupling, following the Spano model.[17,39-41] These properties are found through the ratio of the two identified peaks in Figure 7, $A_{0\text{-}0}$ and $A_{0\text{-}1}$, which are shown to give insight into the relative degrees of intra- and inter-chain order by Equation 2, below:

$$\frac{A_{0-0}}{A_{0-1}} \cong \left(\frac{1 - 0.24W/\hbar\omega_0}{1 + 0.073W/\hbar\omega_0}\right)^2$$

Where W is the free exciton bandwidth, in this case equal to 4 times the cofacial intrachain Coulombic coupling, J_0, assuming the Huang-Rhys factor is 1. Finally, $\hbar\omega_0$ is 180 meV, which is

the energy of the primary vibronic mode associated with electronic transition in P3HT, symmetric ring stretching.[17] As shown in Figure 7, and detailed in Table S1, $A_{0\text{-}0}/A_{0\text{-}1}$ increases with age, indicating that there is more short-range order, *e.g.* backbone planarity and close-packing, in the nanowires as they approach a more thermodynamically limited structure. However, there was still a high degree of defect exclusion observed both for regio-defects and end-groups, which points to a limit in the inclusion of these defects. As such, the extent to which these individual defects can be incorporated into the crystal lattice and the consequences of that inclusion need to be determined.

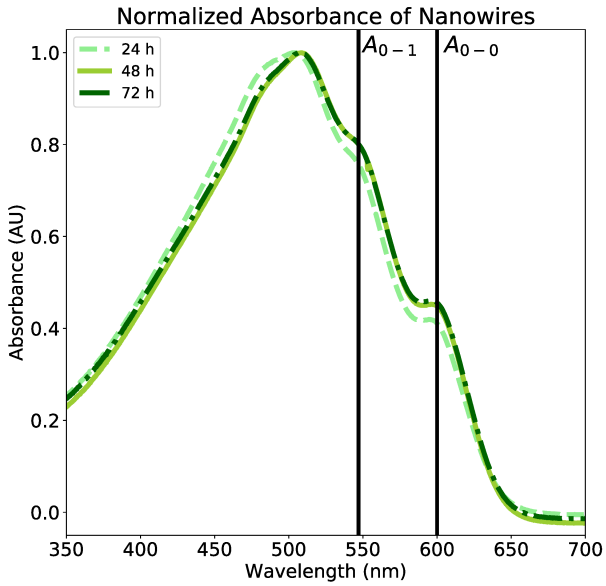

Figure 7. An overlay of the normalized UV-vis absorption spectra for the 24, 48, and 72-hour aged Rieke P3HT nanowires. The absorption peaks corresponding to the 0-0 and 0-1 transitions are marked reference. As seen in above plots, as age increases, so does the $A_{0\text{-}0}/A_{0\text{-}1}$ ratio, signifying more backbone planarity and increased short-range order.

In order to examine the effects of regio-defect incorporation, a series of nanowires made from P3HT with increasing RR were examined, while holding the aging time, molecular weight, $Đ$, and end-groups constant. In these samples, the end-group is Br-H. The results of these experiments are seen in Table S2 and summarized in Figure 8. By increasing the RR of the P3HT from 93% to 99%, $\xi_{(010)}$ was increased by as much as 5-times the original value. Despite this drastic increase in crystalline order, there were still no observed changes in the dimensions of the nanowire or l_c, confirming that the regio-defects were incorporated into crystal lattices. By comparing the two 93% RR nanowires, Table S2 also shows that larger $Đ$ disrupts the crystallization and corresponds to a decrease in $\xi_{(010)}$, further confirming the observation by Roehling *et al*. that nanowire formation preferentially incorporates a narrow $Đ$ of CP to preserve crystalline structure.[38] Although these defects do not alter the dimensions of the nanowire or l_c, their incorporation reduced the hole mobility, μ_h, by almost 2 orders of magnitude, pointing to the disruption of the crystal lattice and short-range order and corroborating our observed trends in $\xi_{(010)}$, shown in Table S2.[17] These experimental results are in keeping with simulations, which have predicted the increase in trap states and paracrystallinity as RR diminishes.[12,42] Therefore, despite the ability of regio-defects to be incorporated into the crystal lattice of CP, there are corresponding distortions of the crystal lattice and reductions in short-range order and optoelectronic properties.

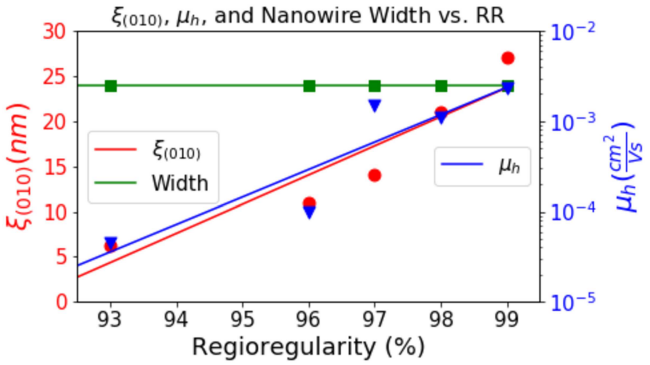

Figure 8: A plot generated from data in Table S2. The hole mobility, nanowire width, and $\xi_{(010)}$ are plotted as a function of regioregularity. Linear fits provide visual guides for the data. Error in the data is associated with instrumental precision. Changes in regioregularity have drastic effects on the short-range order of the nanowires, as measured by both XRD and OFET mobility.

Table S1 indicated that there is a preference to exclude bulky end-groups, but that they are still incorporated into the nanowire. Additionally, there was an observed preference to incorporate P3HT with a DP corresponding to integer multiples of l_c. In order to investigate these trends and the extent to which DP can be used to tune the incorporation of end-groups, a series of nanowires made from highly regioregular P3HT with $Đ$ below 1.3 were made. These P3HT samples were all synthesized with toluene-H end-groups, because the toluene moieties were expected to be able to participate in the π-π interactions of the crystal lattice, which was anticipated to increase the incorporation of the end-groups by decreasing their distortion of the crystal lattice. Further, to investigate the role of DP in the incorporation of end-groups, the nanowires were formed from different P3HT samples with DP corresponding to multiples of the l_c that was noted in Table S1, which was 50 monomer units. The predicted nanowire structures resulting from integer (harmonic) and non-integer (non-harmonic) multiples of 50 monomer units are displayed in Figure 9, the results of the analysis of the nanowires are shown in Table S3.

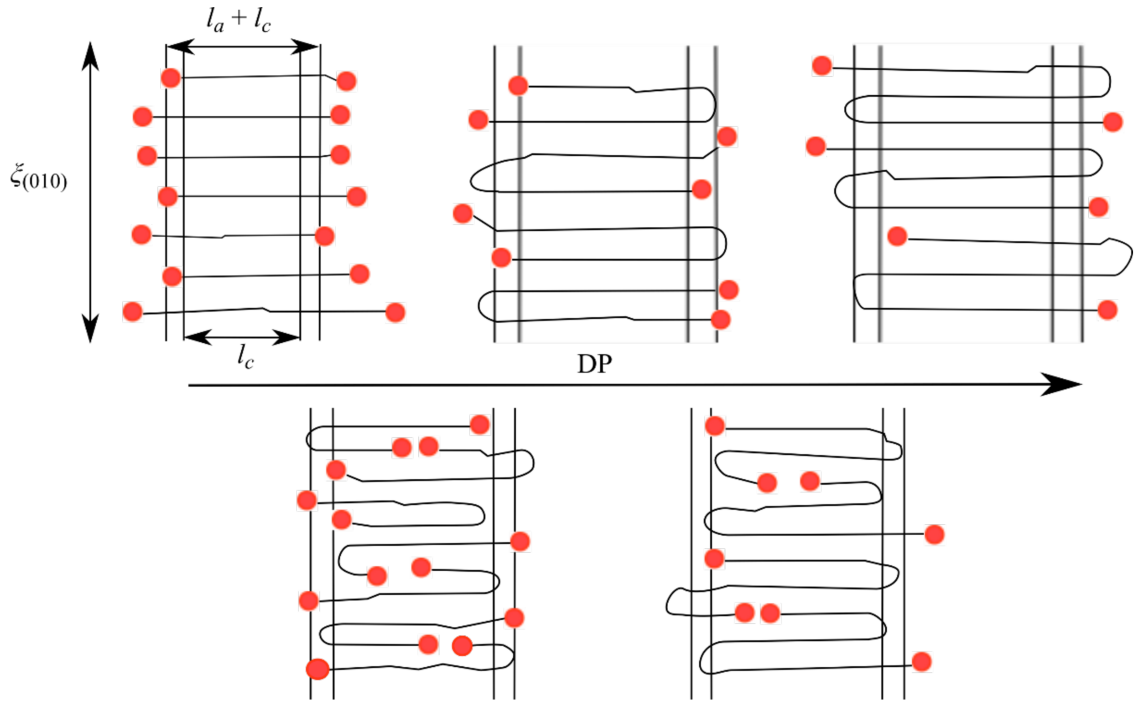

Figure 9. Predicted structures of the nanowires that are described in Table S3, with (top, left to right) DP = 50, 100, 150 and (bottom, left to right) DP = 75, 125. l_c remains relatively consistent for all samples above DP = 50.

The nanowires that had the smallest observed l_c were those made from the DP = 50 P3HT, whose l_c neatly corresponded to the full DP of the P3HT, as shown in Table S3. This smaller l_c is evidenced by the depression of the melting point of the 50 DP nanowires, relative to the other samples, seen in Figure S20. This smaller l_c was in keeping with our predicted structure because 50 DP is at the approximate transition between chain-extended and chain-folded P3HT, so the chains were expected to stack, rather than fold, as shown in Figure 9.[21] As the DP increased beyond 50, the chains folded during nanowire formation and there was a slight increase in the observed l_c of the nanowires, shown in Table S3. This increase is attributed to the ability of π-π interacting toluene end-groups to be incorporated into the crystal lattice, which allows for more monomer units to participate in the lattice, lengthening l_c and, particularly for harmonic DP, increasing ΔH_f, as seen

in Figure 10. We note here that this helps explain the observation made by Koldemir *et al*. that toluene-H capped polymers have stronger aggregation in solution.[28] Because there is less disruption of the crystal lattice and more crystallizable units when toluene-/-H end-groups are used in the nanowires, as opposed to bromine-/-H, CP chains can more strongly interact with each other when π-π interacting end-groups are utilized.

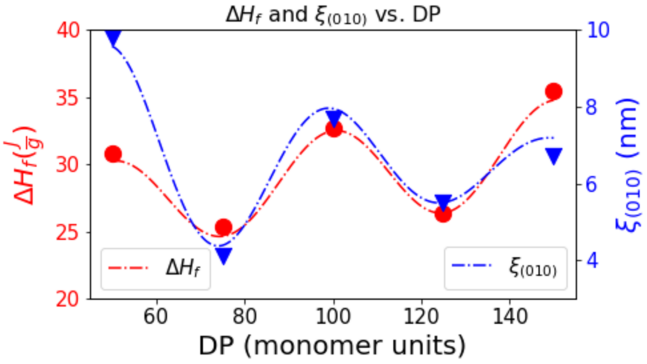

Figure 10: A plot showing the enthalpy of fusion and coherence *versus* DP for a series of P3HT nanowires, described in Table S3. Error in the data is associated with instrumental precision. This plot illustrates the effects of harmonic vs. non-harmonic DP on the crystallinity and short-range order of nanowires. Sinusoidal curves are fitted to emphasize the role of DP on the incorporation of end-groups.

For non-harmonic DP, the l_c also corresponds to our predicted folding patterns, which incorporate the end-groups much more often, thereby decreasing ΔH_f. In the DP = 75 nanowires, the l_c is 67 monomer units, which can be constructed from ~35 monomer unit-long halves of two different chains in the same row. So, with each chain folded into 35 unit halves and ~5 folding units, which are excluded from l_c,[43,44] 35+35+5 = 75, which corresponds to our chain length. The units in the fold of the polymer are excluded from l_c because they are in the all *cis* conformation, which disrupts conjugation in between those units by reducing *p* orbital overlap.[44] This folding structure is

graphically described in Figure 9. Similarly, for P3HT of DP = 125, the l_c is equal to the remaining units of two different chains after folding twice, with 5 folding units in each chain being excluded from l_c, as shown in Figure 9. Because their end-groups cannot be neatly excluded to the nanowire edge, they are incorporated into the lattice and disrupt intermolecular interactions, reducing ΔH_f, so that the long-rang order of the nanowire structure is preserved. Further, because the DP = 125 nanowire has complete folds between the incorporated end-groups, its ΔH_f is larger than the DP = 75 nanowires. As expected, nanowires that incorporate end-groups into the crystal lattice display markedly lower ΔH_f as a result of the lattice distortion introduced by the end-groups and decreasing crystallinity by as much as 20% from nanowires made from P3HT chains that can neatly stack with end-groups at their edges. When the DP is increased from 50 by integer multiples of l_c to 150, the ΔH_f grew from 30.8 to 35.5 J/g. Interestingly, despite the increase of ΔH_f, there was an observed decrease in $\xi_{(010)}$ with larger integer multiples of 50, which is visible in the diminishing (010) peaks in Figures S21-S25 and Figure 10 as DP increases for harmonic DP. This is attributed to the fact that there are more chain folds required for these longer lengths. As the number of required folds increases, the likelihood that a folding or stacking fault occurs also increases, thereby decreasing $\xi_{(010)}$. Because the DP = 50 polymers did not have to fold, it is reasonable that those nanowires have the highest coherence, since crystals grow by first appending the stem and adsorbing units *via* rearranging and 'reeling' in segments to the crystal growth face. Once adsorbed to the width of the growth face, the remaining polymer folds to adsorb, creating more opportunities for crystallographic faults.[45,46]

So far, we have demonstrated that defects in the chemical structure of P3HT can be incorporated into the crystal lattice, but that the type of defect and its steric bulk influence the extent of its disruption of the crystallization and final structure. Specifically, polymer chains with <10% regio-

defects and aromatic end-groups are readily incorporated into the crystal lattice. In general, we have also seen that the presence of defects frustrates crystallization, with bulkier defects being excluded to a greater extent because they reduce structural coherence and short-range order more severely. As a result, defects that can interact favorably with the lattice are more readily incorporated and can be used to modify and promote short-range order, as with the toluene end-groups. To directly observe these effects, we formed nanowires from 3 different P3HT samples and probed their structure using amplitude-modulated, frequency-modulated (AMFM) force microscopy, a bimodal AFM technique that is capable of simultaneously measuring the Young's modulus (E) of a material and topography with a resolution on the 10 nanometer scale (Figure 11).[47,48] AMFM has previously been used to distinguish between crystalline and amorphous regions of P3HT thin films.[49] In order to distinguish the different polymer samples, they will be referred to by their defect types and concentration following the convention: (end-group)-(DP)-(RR)-(dispersity). So, Tol-200-100-narrow has the lowest defect concentration with toluene-H end-groups, a DP of 200 (an integer multiple of l_c), RR = 100%, and a narrow $Đ$ of 1.1. Br-275-98-narrow has a slightly higher defect concentration, having bulkier Br-H end-groups, a DP = 275 (a non-integer multiple of l_c), RR = 98%, and with a narrow $Đ$ of 1.2. Finally, Br-150-91-wide is commercially available P3HT with a higher concentration of defects, having Br-H end-groups, a DP of 150, RR = 91%, but with a wide $Đ$ of 1.8.

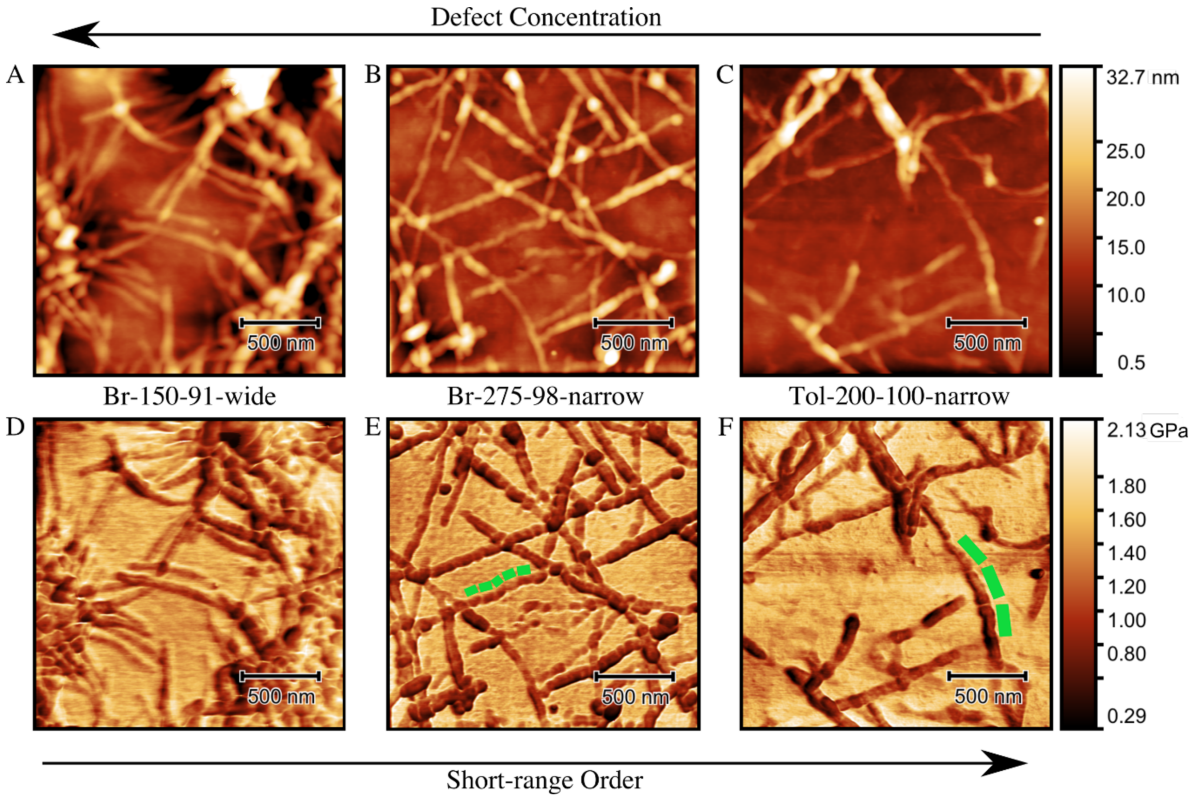

Figure 11. (A-C) 2x2 μm topographical scans of nanowires formed from Tol-200-100-narrow, Br-275-98-narrow, and Br-150-91-wide (right-to-left). (D-F) Young's modulus scans of the same nanowires. All images are from AMFM scans, all scale-bars are 500 nm. Larger segments are seen in nanowires made from P3HT with lower defect concentrations and π-interacting end-groups. As indicated, defect concentration increases from right-to-left, and short-range order increases from left-to-right. The length of segments, or crystal grains, in the nanowires are denoted in Figure 11 E and F with green rectangles. Grain size increases as defect concentration is reduced.

The topography scans (Figure 11, A-C) show nanowires with similar dimensions between each sample, however, the nanostructure of the nanowires is different for each sample. Tol-200-100-narrow nanowires exhibit large crystal grains in many different nanowires, which are represented with green rectangles in Figure 11 F. Br-275-98-narrow nanowires also show crystal grains in many of its nanowires, also highlighted with green rectangles in Figure 11 E, but these appear

much smaller than those shown in the Tol-200-100-narrow sample. While there are visible grain segments at these low defect concentrations, there are no discernible crystal grains in the Br-150-91-wide nanowires. In fact, the nanowires in Figure 11 A and D are remarkably homogeneous. The root-mean-square roughness (r_{rms}) of line-scans along the nanowires' long-axis reflects these observations. The Br-150-91-wide nanowires had the smallest r_{rms} variation in both height and modulus, (0.3 ± 0.1 nm, and 0.05 ± 0.01 GPa variation) these nanowires have few distinguishable structure features along their backbones. Tol-200-100-narrow nanowires were the next smoothest (rms roughness in height 0.4 ± 0.1 nm and rms variation in modulus 0.08 ± 0.008 GPa). These nanowires had the larger crystal grains and some fluctuations in the *E* within the grains. Finally, the Br-275-98-narrow had similar r_{rms} in height, but the largest variation in modulus (0.4 ± 0.2 nm and 0.09 ± 0.03 GPa). This follows, as the Br-275-98-narrow nanowires have smaller segments and, correspondingly, more grain boundaries, as well as some fluctuations in *E* within the nanowire segments. The differences in nanowire structure are ascribed to two main effects of the defects– slowing crystal growth and the disruption of short-range order. As examined above, the incorporation of defects slows down crystal growth by reducing the inter-chain interactions of crystallizing stems.[46,50] Since the NWs grow from the end by attaching stems, the termination of a grain would come from either the lack of stems with low enough defect concentration to participate in crystallization, or the presence of defects and the leading edge frustrating further stem appending.[45,46] So, following this, the area between the grains corresponds to a thin bridging layer of P3HT that was still able to crystallize. This description is confirmed by observing that the height of these inter-grain domains are ~2 nm, which corresponds to 1 vertical layer of P3HT.[44]

Of the three imaged polymers, Tol-200-100-narrow had the fewest defects to incorporate, so its nanowire growth was minimally disrupted, short-range order remained high, and large grains were

able to grow. Br-275-98-narrow also had relatively few defects, but its DP was non-harmonic, so the bulky Br end-groups were forced to incorporate more often into the nanowire structure. As a result, the grain growth was interrupted more often, and the grains were correspondingly smaller. Finally, the Br-150-91-wide had a high concentration of regio-defects, bulky end-groups, and a large $Đ$. This means that its crystal grain growth was slow because it was interrupted by defects often. As a result, the coherence in the [010] direction is minimized and any boundaries between the small grains are nearly indistinguishable from the rest of the nanowire.

These differences in nanowire structures are more clearly visible in Figure 11 D-F, which show the corresponding E scans of the nanowires. These scans are essentially a measure of the strength of the intermolecular interactions in the nanowires, which can be used to evaluate and describe differences in the local crystallinity of the polymer.[51,52] As noted above, the Br-150-91-wide nanowires are much more homogenous than the other two samples, resulting from the slow and frustrated crystal growth. Conversely, the Br-275-98-narrow nanowires are largely dark ($E \approx 1.0$ GPa) but have noticeable lighter grains ($E \approx 1.5$ GPa) and areas within the grains. Similarly, the Tol-200-100-narrow nanowires have visible fluctuations in E between grains and within each grain. Because differences in modulus of P3HT result from varied intermolecular interactions, these differences in modulus also correspond to local variations in the ΔH_f of the crystal. The fluctuations within the nanowire grains in Figures 11 E and F are seen more than just parallel to the scan direction of these images, which is horizontal. Because they occur along many different axes, we can conclude that the local fluctuations in ΔH_f are not solely from tip-surface interactions. Instead, they are local disruptions in short-range order, presumably as a result of defect inclusion into the crystal lattice. The largest fluctuations in E occur between crystal segments of the same nanowire, at the grain boundaries. These bridging layers are shown to be stiffer than the nanowire

bulk in Figures S26-S28. The increased stiffness arises both because a reduction in thickness tends to increase modulus and because the grains incorporated defects to a point where crystal growth was stymied, and only the crystalline bridging layer was able to grow.[53,54] So, the *E* of the grain is diminished by the defect incorporation, while the bridging layer retains a less-distorted and stiffer lattice. These observations on the impact of defects and crystallization on the short-range order and material properties of CP are reinforced by the UV-vis analysis of the imaged polymers, as shown in Figure 12. The calculated $A_{0\text{-}0}/A_{0\text{-}1}$ values were 0.75 for Tol-200-100-narrow, 0.74 for Br-275-98-narrow, and 0.66 for Br-150-91-wide. As short-range order increased, the optoelectronic properties are improved through increased planarity and orbital overlap. These results demonstrate that there is inclusion of defects into lattices and that this inclusion results in the noted differences in crystal growth and short-range order, confirming the results of Tables S1-S3. Interestingly, despite these differences and widely varied defect concentrations, each of these polymers was able to self-assemble into nanowires and maintain long-range order. This points to a preference of CP to sacrifice short-range order to maintain long-range and structural order.

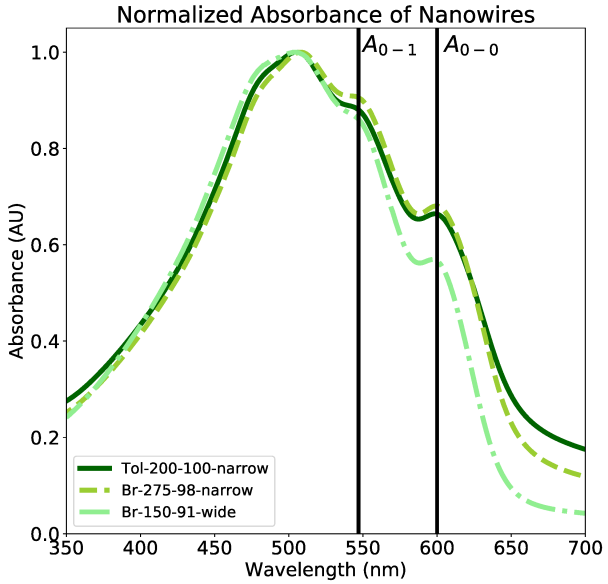

Figure 12. An overlay of the UV-vis absorption profiles for the nanowires shown in Figure 11. The absorption peaks corresponding to the 0-0 and 0-1 electronic transitions are marked for reference. An increase in the $A_{0\text{-}0}/A_{0\text{-}1}$ ratio signifies increased short-range order and electronic coherence along the backbone. As discussed, Br-150-91-wide had the most defects, least order and, correspondingly the lowest $A_{0\text{-}0}/A_{0\text{-}1}$ ratio. Conversely, Tol-200-100-narrow had the fewest overall defects and therefore has the highest $A_{0\text{-}0}/A_{0\text{-}1}$ ratio.

CONCLUSIONS

It has been demonstrated that both regio-defects and end-groups can be partially incorporated into the crystal lattice of CPs and that this incorporation disrupts structural coherence and short-range order. Regio-defects can be included at concentrations as high as 10%, although this comes at the cost of decreasing both the charge mobility of the nanowires and ΔH_f of the crystallites. This may parallel the observation that CPs have been shown to have high paracrystallinity, even in films that are highly crystalline and well aligned.[55] In other words, regio-defects may affect the crystal lattice to the same degree as typical cumulative disorder, which is highly tolerated by the crystal lattice of CP. It has also been demonstrated that end-groups can be incorporated into the crystal lattice, although there is a strong preference to exclude them. Particularly in the case of Br, the steric bulk of the end-groups severely disrupts the crystal lattice. Importantly, our results reveal that end-groups can be selected to participate more easily in the crystal lattice. By choosing small end-groups, their incorporation can occur with a significantly reduced enthalpic penalty. Further, by selecting end-groups that can participate in π-π interactions, such as toluene, the lattice distortions resulting from the end-group incorporation can be mitigated and long-range order can be promoted. This underscores the importance of considering the identity of end-groups during the

design of a polymer for a given application, where morphology and crystallinity can directly affect device performance, such as with OFET and OPV.

Our results have also pointed to another route to mitigate the inclusion of end-groups, which is to 'tune' the DP of the polymer to be equal to an integer multiple of the observed l_c. By doing so, chain-folding ensures that the end-group will be located at the edge of the crystalline domain and thereby increase the crystallinity of the nanowire by as much as 20%. This observation is expected to be translatable to thin film active layers for optoelectronic devices, and is anticipated to prove particularly effective in devices that have their active layers deposited through techniques like blade-coating, which align polymer chains into highly crystalline and nano-structured thin films *via* sheer force, because of their structural similarity to nanowires.

Supporting Information

Materials, experimental methods, poly(3-hexylthiophene) characterization info, calorimetry data, X-ray diffraction data, example AFM micrographs. This file is available free of charge.

Corresponding Author

* E-mail: luscombe@uw.edu

Funding Sources

The authors declare no competing financial interest.

Acknowledgements

The authors acknowledge NSF DMR-1708317 for funding. DSG and LQF acknowledge support of the AMFM polymer imaging by NSF DMR-1607242. Part of this work was conducted at the Molecular Analysis Facility, a National Nanotechnology Coordinated Infrastructure site at the University of Washington which is supported in part by the National Science Foundation (grant

ECCS-1542101), the University of Washington, the Molecular Engineering & Sciences Institute, and the Clean Energy Institute.

REFERENCES

(1) Zhou, H.; Yang, L.; You, W. Rational Design of High Performance Conjugated Polymers for Organic Solar Cells. *Macromolecules* **2012**, *45* (2), 607–632.

(2) Morin, P.-O.; Bura, T.; Leclerc, M. Realizing the Full Potential of Conjugated Polymers: Innovation in Polymer Synthesis. *Mater. Horizons* **2016**, *3* (1), 11–20.

(3) Li, Y.; Tatum, W. K.; Onorato, J. W.; Zhang, Y.; Luscombe, C. K. Low Elastic Modulus and High Charge Mobility of Low-Crystallinity Indacenodithiophene-Based Semiconducting Polymers for Potential Applications in Stretchable Electronics. *Macromolecules* **2018**, *51* (16), 6352–6358.

(4) Patel, S. N.; Glaudell, A. M.; Kiefer, D.; Chabinyc, M. L. Increasing the Thermoelectric Power Factor of a Semiconducting Polymer by Doping from the Vapor Phase. *ACS Macro Lett.* **2016**, *5* (3), 268–272.

(5) Zhang, C.; Wang, Y.; Cheng, S.; Zhang, X.; Fu, B.; Hu, W. Assembly of π-Conjugated Nanosystems for Electronic Sensing Devices. *Adv. Electron. Mater.* **2017**, *3* (11), 1700209.

(6) Li, S.; Ye, L.; Zhao, W.; Yan, H.; Yang, B.; Liu, D.; Li, W.; Ade, H.; Hou, J. A Wide Band Gap Polymer with a Deep Highest Occupied Molecular Orbital Level Enables 14.2% Efficiency in Polymer Solar Cells. *J. Am. Chem. Soc.* **2018**, *140* (23), 7159–7167.

(7) Holliday, S.; Li, Y.; Luscombe, C. K. Recent Advances in High Performance Donor-

Acceptor Polymers for Organic Photovoltaics. *Prog. Polym. Sci.* **2017**, *70*, 34–51.

(8) Holliday, S.; Donaghey, J. E.; McCulloch, I. Advances in Charge Carrier Mobilities of Semiconducting Polymers Used in Organic Transistors. *Chem. Mater.* **2014**, *26* (1), 647–663.

(9) Bronstein, H. A.; Luscombe, C. K. Externally Initiated Regioregular P3HT with Controlled Molecular Weight and Narrow Polydispersity. *J. Am. Chem. Soc.* **2009**, *131* (36), 12894–12895.

(10) Huang, Y.; Luscombe, C. K. Towards Green Synthesis and Processing of Organic Solar Cells. *Chem. Rec.* **2019**, *19*, 1–12.

(11) Mauer, R.; Kastler, M.; Laquai, F. The Impact of Polymer Regioregularity on Charge Transport and Efficiency of P3HT:PCBM Photovoltaic Devices. *Adv. Funct. Mater.* **2010**, *20* (13), 2085–2092.

(12) Poelking, C.; Andrienko, D. Effect of Polymorphism, Regioregularity and Paracrystallinity on Charge Transport in Poly(3-Hexylthiophene) [P3HT] Nanofibers. *Macromolecules* **2013**, *46* (22), 8941–8956.

(13) Kim, J.-S.; Kim, J.-H.; Lee, W.; Yu, H.; Kim, H. J.; Song, I.; Shin, M.; Oh, J. H.; Jeong, U.; Kim, T.-S.; et al. Tuning Mechanical and Optoelectrical Properties of Poly(3-Hexylthiophene) through Systematic Regioregularity Control. *Macromolecules* **2015**, *48* (13), 4339–4346.

(14) Snyder, C. R.; Henry, J. S.; Delongchamp, D. M. Effect of Regioregularity on the Semicrystalline Structure of Poly(3-Hexylthiophene). *Macromolecules* **2011**, *44*, 7088–

7091.

(15) Kohn, P.; Huettner, S.; Komber, H.; Senkovskyy, V.; Tkachov, R.; Kiriy, A.; Friend, R. H.; Steiner, U.; Huck, W. T. S.; Sommer, J.-U.; et al. On the Role of Single Regiodefects and Polydispersity in Regioregular Poly(3-Hexylthiophene): Defect Distribution, Synthesis of Defect-Free Chains, and a Simple Model for the Determination of Crystallinity. *J. Am. Chem. Soc.* **2012**, *134* (4790–4805), 4790–4805.

(16) Balar, N.; O'Connor, B. T. Correlating Crack Onset Strain and Cohesive Fracture Energy in Polymer Semiconductor Films. *Macromolecules* **2017**, *50* (21), 8611–8618.

(17) Mazzio, K. A.; Rice, A. H.; Durban, M. M.; Luscombe, C. K. Effect of Regioregularity on Charge Transport and Structural and Excitonic Coherence in Poly(3-Hexylthiophene) Nanowires. *J. Phys. Chem. C* **2015**, *119* (27), 14911–14918.

(18) Baghgar, M.; Labastide, J.; Bokel, F.; Dujovne, I.; Mckenna, A.; Barnes, A. M.; Pentzer, E.; Emrick, T.; Hayward, R.; Barnes, M. D. Probing Inter-and Intrachain Exciton Coupling in Isolated Poly(3- Hexylthiophene) Nanofibers: Effect of Solvation and Regioregularity. *J. Phys. Chem. Lett* **2012**, *3*, 1674–1679.

(19) Shimomura, T.; Takahashi, T.; Ichimura, Y.; Nakagawa, S.; Noguchi, K.; Heike, S.; Hashizume, T. Relationship between Structural Coherence and Intrinsic Carrier Transport in an Isolated Poly(3-Hexylthiophene) Nanofiber. *Phys. Rev. B* **2011**, *83* (11), 115314.

(20) Koch, F. P. V.; Rivnay, J.; Foster, S.; Müller, C.; Downing, J. M.; Buchaca-Domingo, E.; Westacott, P.; Yu, L.; Yuan, M.; Baklar, M.; et al. The Impact of Molecular Weight on Microstructure and Charge Transport in Semicrystalline Polymer Semiconductors–Poly(3-

Hexylthiophene), a Model Study. *Prog. Polym. Sci.* **2013**, *38* (12), 1978–1989.

(21) Snyder, C. R.; Nieuwendaal, R. C.; DeLongchamp, D. M.; Luscombe, C. K.; Sista, P.; Boyd, S. D. Quantifying Crystallinity in High Molar Mass Poly(3-Hexylthiophene). *Macromolecules* **2014**, *47* (12), 3942–3950.

(22) Zhugayevych, A.; Mazaleva, O.; Naumov, A.; Tretiak, S. Lowest-Energy Crystalline Polymorphs of P3HT. *J. Phys. Chem. C* **2018**, *122* (16), 9141–9151.

(23) Baghgar, M.; Labastide, J. A.; Bokel, F.; Hayward, R. C.; Barnes, M. D. Effect of Polymer Chain Folding on the Transition from H- to J-Aggregate Behavior in P3HT Nanofibers. *J. Phys. Chem. C* **2014**, *118* (4), 2229–2235.

(24) Kim, S.; Park, J. K.; Park, Y. D. Charge Transport Behaviors of End-Capped Narrow Band Gap Polymers in Bottom-Contact Organic Field-Effect Transistors. *RSC Adv.* **2014**, *4* (74), 39268–39272.

(25) Onorato, J. W.; Luscombe, C. K. Morphological Effects on Polymeric Mixed Ionic/Electronic Conductors. *Mol. Syst. Des. Eng.* **2019**, *4* (2), 310–324.

(26) Dong, B. X.; Nowak, C.; Onorato, J. W.; Strzalka, J.; Escobedo, F. A.; Luscombe, C. K.; Nealey, P. F.; Patel, S. N. Influence of Side-Chain Chemistry on Structure and Ionic Conduction Characteristics of Polythiophene Derivatives: A Computational and Experimental Study. *Chem. Mater.* **2019**, acs.chemmater.8b05257.

(27) Flagg, L. Q.; Bischak, C. G.; Onorato, J. W.; Rashid, R. B.; Luscombe, C. K.; Ginger, D. S. Polymer Crystallinity Controls Water Uptake in Glycol Side-Chain Polymer Organic Electrochemical Transistors. *J. Am. Chem. Soc.* **2019**, *141* (10), 4345–4354.

(28) Koldemir, U.; Puniredd, S. R.; Wagner, M.; Tongay, S.; McCarley, T. D.; Kamenov, G. D.; Müllen, K.; Pisula, W.; Reynolds, J. R. End Capping Does Matter: Enhanced Order and Charge Transport in Conjugated Donor–Acceptor Polymers. *Macromolecules* **2015**, *48* (18), 6369–6377.

(29) Flory, P. J. Theory of Crystallization in Copolymers. *Trans. Faraday Soc.* **1955**, *51* (0), 848.

(30) Sanchez, I. C.; Eby, R. K. Thermodynamics and Crystallization of Random Copolymers. *Macromolecules* **1975**, *8* (5), 638–641.

(31) Yasuniwa, M.; Haraguchi, K.; Nakafuku, C.; Hirakawa, S. Effect of Molecular Weight on the Phase Diagram of Polyethylene under High Pressure. *Polym. J.* **1985**, *17* (11), 1209–1219.

(32) Wang, Z.; Ju, J.; Yang, J.; Ma, Z.; Liu, D.; Cui, K.; Yang, H.; Chang, J.; Huang, N.; Li, L. The Non-Equilibrium Phase Diagrams of Flow-Induced Crystallization and Melting of Polyethylene. *Sci. Rep.* **2016**, *6* (1), 32968.

(33) He, P. The Distribution of Degree of Crystallinity—New Concept in Polymer Science. *Chinese Chem. Lett.* **2018**, *29* (12), 1711–1712.

(34) Yang, Y.; Chen, M.; Li, H.; Li, H. The Degree of Crystallinity Exhibiting a Spatial Distribution in Polymer Films. *Eur. Polym. J.* **2018**, *107*, 303–307.

(35) Chiu, M.; Jeng, U.; Su, C.; Liang, K. S.; Wei, K. Simultaneous Use of Small- and Wide-Angle X-ray Techniques to Analyze Nanometerscale Phase Separation in Polymer Heterojunction Solar Cells. *Adv. Mater.* **2008**, *20* (13), 2573–2578.

(36) Hosemann, R. Crystalline and Paracrystalline Order in High Polymers. *J. Appl. Phys.* **1963**, *34* (1), 25–41.

(37) Tatum, W. K.; Luscombe, C. K. π-Conjugated Polymer Nanowires: Advances and Perspectives toward Effective Commercial Implementation. *Polym. J.* **2018**, *50* (8), 659–669.

(38) Roehling, J. D.; Arslan, I.; Moulé, A. J. Controlling Microstructure in Poly(3-Hexylthiophene) Nanofibers. *J. Mater. Chem.* **2012**, *22* (6), 2498.

(39) Hestand, N. J.; Spano, F. C. Expanded Theory of H- and J-Molecular Aggregates: The Effects of Vibronic Coupling and Intermolecular Charge Transfer. *Chem. Rev.* **2018**, *118* (15), 7069–7163.

(40) Spano, F. C.; Silva, C. H- and J-Aggregate Behavior in Polymeric Semiconductors. *Annu. Rev. Phys. Chem.* **2014**, *65* (1), 477–500.

(41) Yamagata, H.; Spano, F. C. Interplay between Intrachain and Interchain Interactions in Semiconducting Polymer Assemblies: The HJ-Aggregate Model. *J. Chem. Phys.* **2012**, *136* (18), 184901.

(42) McMahon, D. P.; Cheung, D. L.; Goris, L.; Dacuña, J.; Salleo, A.; Troisi, A. Relation between Microstructure and Charge Transport in Polymers of Different Regioregularity. *J. Phys. Chem. C* **2011**, *115* (39), 19386–19393.

(43) Mena-Osteritz, E.; Meyer, A.; Langeveld-Voss, B. M. W.; Janssen, R. A. J.; Meijer, E. W.; Bäuerle, P. Two-Dimensional Crystals of Poly(3-Alkyl- Thiophene)s: Direct Visualization of Polymer Folds in Submolecular Resolution. *Angew. Chemie Int. Ed.* **2000**, *39* (15), 2679–

2684.

(44) Han, Y.; Guo, Y.; Chang, Y.; Geng, Y.; Su, Z. Chain Folding in Poly(3-Hexylthiophene) Crystals. *Macromolecules* **2014**, *47* (11), 3708–3712.

(45) Welch, P.; Muthukumar, M. Molecular Mechanisms of Polymer Crystallization from Solution. *Phys. Rev. Lett.* **2001**, *87* (21), 218302.

(46) Verho, T.; Paajanen, A.; Vaari, J.; Laukkanen, A. Crystal Growth in Polyethylene by Molecular Dynamics: The Crystal Edge and Lamellar Thickness. *Macromolecules* **2018**, *51* (13), 4865–4873.

(47) Garcia, R.; Proksch, R. Nanomechanical Mapping of Soft Matter by Bimodal Force Microscopy. *Eur. Polym. J.* **2013**, *49* (8), 1897–1906.

(48) Herruzo, E. T.; Garcia, R. Theoretical Study of the Frequency Shift in Bimodal FM-AFM by Fractional Calculus. *Beilstein J. Nanotechnol.* **2012**, *3* (1), 198–206.

(49) Giridharagopal, R.; Flagg, L. Q.; Harrison, J. S.; Ziffer, M. E.; Onorato, J.; Luscombe, C. K.; Ginger, D. S. Electrochemical Strain Microscopy Probes Morphology-Induced Variations in Ion Uptake and Performance in Organic Electrochemical Transistors. *Nat. Mater.* **2017**, *16* (7), 737–742.

(50) Pulst, M.; Schneemann, C.; Ruda, P.; Golitsyn, Y.; Grefe, A.-K.; Stühn, B.; Busse, K.; Reichert, D.; Kressler, J. Chain Tilt and Crystallization of Ethylene Oxide Oligomers with Midchain Defects. *ACS Macro Lett.* **2017**, *6* (11), 1207–1211.

(51) Nguyen, H. K.; Ito, M.; Nakajima, K. Elastic and Viscoelastic Characterization of

Inhomogeneous Polymers by Bimodal Atomic Force Microscopy. *Jpn. J. Appl. Phys.* **2016**, *55* (8S1), 08NB06-1 – 7.

(52) Kocun, M.; Labuda, A.; Meinhold, W.; Revenko, I.; Proksch, R. Fast, High Resolution, and Wide Modulus Range Nanomechanical Mapping with Bimodal Tapping Mode. *ACS Nano* **2017**, *11* (10), 10097–10105.

(53) Christopher M. Stafford, *,†; Bryan D. Vogt, †; Christopher Harrison, †,§; Duangrut Julthongpiput, †,⊥ and; Huang‡, R. Elastic Moduli of Ultrathin Amorphous Polymer Films. **2006**.

(54) Saha, R.; Nix, W. D. Effects of the Substrate on the Determination of Thin Film Mechanical Properties by Nanoindentation. *Acta Mater.* **2002**, *50* (1), 23–38.

(55) Noriega, R.; Rivnay, J.; Vandewal, K.; V Koch, F. P.; Stingelin, N.; Smith, P.; Toney, M. F.; Salleo, A. A General Relationship between Disorder, Aggregation and Charge Transport in Conjugated Polymers. *Nat. Mater.* **2013**, *12*, 1038–1044.